# Internal Structure Models for Hypothetical Icy Exoplanet

**PHY 304 2.0**

**By,**

**S R Wijendra**

# *Table of Contents*


1 Introduction ..... 5

1.1 Background study and exoplanet detection ..... 5

1.2 Mass – Radius Relationship ..... 7

1.3 Chemical and elemental abundance ..... 8

1.3.1 Super Earths and Exoplanets ..... 8

1.3.2 Bulk composition and chemical formation ..... 9

1.3.3 Different compositions layer wise ..... 10

1.4 Equation of State ..... 12

1.5 Numerical model ..... 15

2 Methodology ..... 16

2.1 Bulk composition and phase transition ..... 17

2.2 Numerical Modelling ..... 18

3 Results ..... 23

3.1 Rocky Planetary Models ..... 23

3.1.1 Completed script for Earth. 4.4.1 ..... 23

3.1.2 Completed script for Venus. ..... 23

3.2 Ice Planetary Models ..... 24

3.2.1 Completed script 01. (Figure 4.3.1: a) ..... 24

3.2.2 Completed script 02. (Figure 4.3.2: a) ..... 25

3.2.3 Incomplete Script 01. ..... 25

3.3 Icy exoplanet and Rocky planet Comparison. ..... 25

4 Discussion and conclusion ..... 26

4.1 Assumptions of chemical composition and bulk composition with respect to each layer. 26

4.1.1 Chemical composition in core layer ..... 26

4.1.2 Chemical composition in mantle ..... 27

4.1.3 Chemical and bulk composition in ice/water layer ..... 27

4.1.4 Bulk composition assumptions ..... 28

4.2 EoS and its pressure ranges, alternative EoS and the benefits over them. ..... 28

4.3 Readings ..... 29

4.3.1 Completed Ice model 01 (Table 3.2.1: a) ..... 29

4.3.2 Completed Ice model 02. (Table 3.2.2: a) ..... 30

4.3.3 Incomplete Ice model 01. (Table 3.2: c. Ice model 03, properties (incomplete)) ... 31

4.3.4 Ice model and Rocky model comparison. (Table 3.3: a. Comparison of ice model and rocky model.) ..... 31

4.4 Modelling rocky model for earth, Mercury, Venus, Mars. (Accuracy of model) ..... 31

4.4.1 Earth interior structure test. (Completed script for Earth. 4.4.1) ..... 31

4.4.2 Venus interior structure test (Completed script for Venus). ..... 32

4.5 Improvements on script. ..... 32

5 Bibliography ..... 32

6 Appendix ..... 35

6.1 Incomplete models of exoplanets. ..... 35

# *Table of Figures*

Table 1.4:a. **The thermoelastic data of Mg-perovskite (MgSiO3, pv) for different EOS**, for low pressure regions in upper mantle and crust perovskite thermoelastic data can be used. Basically, these values are accurate for low pressure ranges below 200GPa which means all the laboratory conditions have confirmed these values according to Birch Murnaghan EoS (Hakim, 2014). .... 12

Table 1.4:b. **The thermoelastic data of Mg-post-perovskite (MgSiO3, ppv) for different EOS.**, for slightly high-pressure regions in lower mantle post-perovskite thermoelastic data can be used. Basically, these values are accurate for low pressure ranges below 200GPa which means all the laboratory conditions have confirmed these values according to Birch Murnaghan EoS. These values suit on ice/water script using 3rd order Birch-Murnaghan as the EoS (Hakim, 2014)..... 13

Table 1.4:c **The thermoelastic data of ε-Fe for different equations of state,** for the modelling of core layer, thermoelastic data according the Bouchet EoS is going to be used to solve ODEs. (Hakim, 2014). ..... 15

Table 1.5:a. **The modelling strategy is depicted schematically**. Shades of blue represent density calculations, while shades of orange represent ODEs. Each model has two distinct components: composition and structure. They are used as input for the integration of the five ordinary differential equations (ODE), which are radial mass, radial pressure, radial temperature, radial gravity, and heat flux. The five ODEs are solved together by specifying appropriate boundary and continuity conditions. This modelling produces planetary radial profiles of gravity, pressure, temperature, mass, heat flux, and density. In addition, suitable equations of state (EOS) for the mantle, core, and rest must be determined. ..... 16

Table 3.1:a. Completed model for earth structure. ..... 23

Table 3.1:b. Completed two model's data for Venus structure. ..... 24

Table 3.2:a. Ice model 01, properties ..... 25

Table 3.2:b. Ice model 02, properties ..... 25

Table 3.2:c. Ice model 03, properties (incomplete) ..... 25

3.3:a. Icy exoplanet, Rocky planet comparison chart. ..... 26

Figure 4.3:a. Temperature profile for completed ice model 01. ..... 29

Figure 4.3:b. Pressure profile for completed ice model 01. ..... 30

Figure 4.3:c. Temperature profile for completed ice model 02. ..... 30

Figure 4.3:d. Pressure profile for completed ice model 02. ..... 31

Table 6.1:a. This model consists ice 10 layer soon after the silicate mantle and then on the top of ice 10 layer there is a water layer. Final physical properties are taken after the end of water layer which means soon after the water layer it may exists atmosphere or else. ..... 35

6.1:b. This model starts ice layer from Upper mantle, MCB. This consists Ice 06 layer up to the end of the planet. ..... 35

6.1:c. Ice layer starts with Ice 07 on this model. This ice 7 layer starts with Lower mantle, MCB layer. ..... 36

6.1:d. This model ends with ice 07 layer and then water layer. As most of the generated models, this ice layers are start-up with Lower mantle, MCB layer. ..... 36

6.1:e. Model ends with ice 07 layer which starts from Lower mantle, MCB layer. ..... 36

6.1:f. Thermoelastic properties of different elements according to the Chemical abundance of the planet. These values are used to obtain bulk properties on EoS solving. (Assumptions of chemical composition and bulk composition with respect to each layer.) ..... 36

# 1 Introduction

## 1.1 Background study and exoplanet detection

The number of exoplanets discovered has risen dramatically since the start of space missions dedicated to the quest for planets beyond our Solar System, such as NASA's Kepler project. Approximately 4380 planets have been confirmed (brenen, et al., 2021), with thousands more awaiting confirmation. After the first observation of a planet orbiting a star other than the Sun, the field of comparative exoplanetology has rapidly expanded due to the increasing number of observed exoplanets. More than one-third of the known exoplanets lie in orbits smaller than the Mercury's orbit where no Solar System planet exists, with more likely to be discovered by space missions or ground-based surveys.

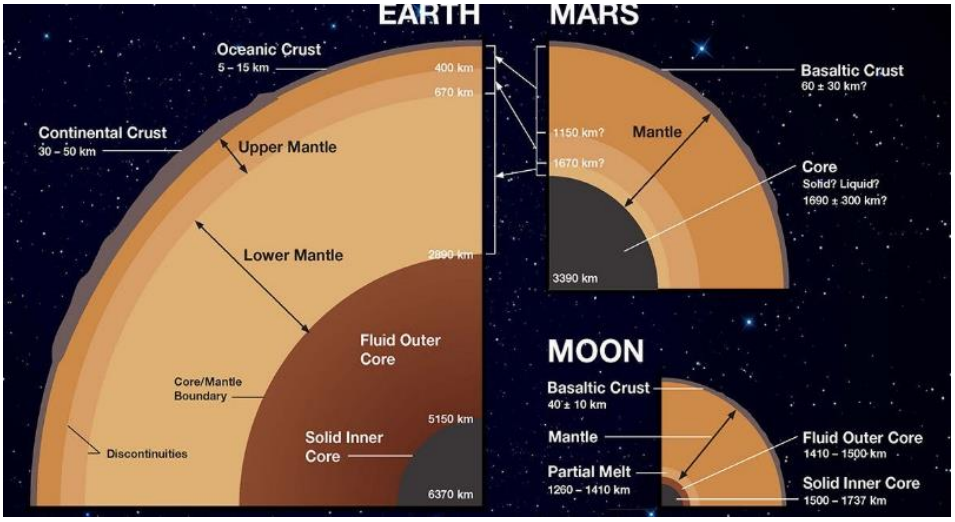


*Figure 1.1:a.* ***EARTH'S INTERIOR STRUCTURES, MARS' INTERIOR STRUCTURES, AND THE MOON'S INTERIOR STRUCTURES,*** *the layered structure of all terrestrial planets is three-parts. A metallic, iron-rich core, part of which may be molten, sits at the middle. The mantle, which makes up most of the planet's mass, is a dense middle layer made of silicate rock (composed mostly of silicon, oxygen, iron, and magnesium) that lies above the core. A thin crust of less dense rocky material remains above the mantle. The crust contains more lighter elements than the mantle (aluminium, sodium, calcium, and sulphur) (Murray, 2018).*

The transit method has been used to detect most exoplanets. When a planet passes from the viewer to the star in the direction, it blocks part of the star-emitted light. This plunge in the star's light curve can be measured by a precise photometer. The radius of the planet can then be inferred if the radius of the star can be determined. Exoplanets are detected by observation of small changes in the Earth's radial velocity of a star. This Radial Velocity method is based on the principle that

if the orbital plane is not perpendicular to the line of sight, the star with an exoplanet is orbiting around the common centre of mass and thus periodically move from and to ourselves. This motion can be detected through blue and redshifts of the stellar spectrum. Other than these two methods Direct imaging and gravitational micro lensing techniques are used to define exoplanets (Fischer, et al., 2011).

Terrestrial planets are structures excluding Mars, Venus, and Mercury that are mostly made up of

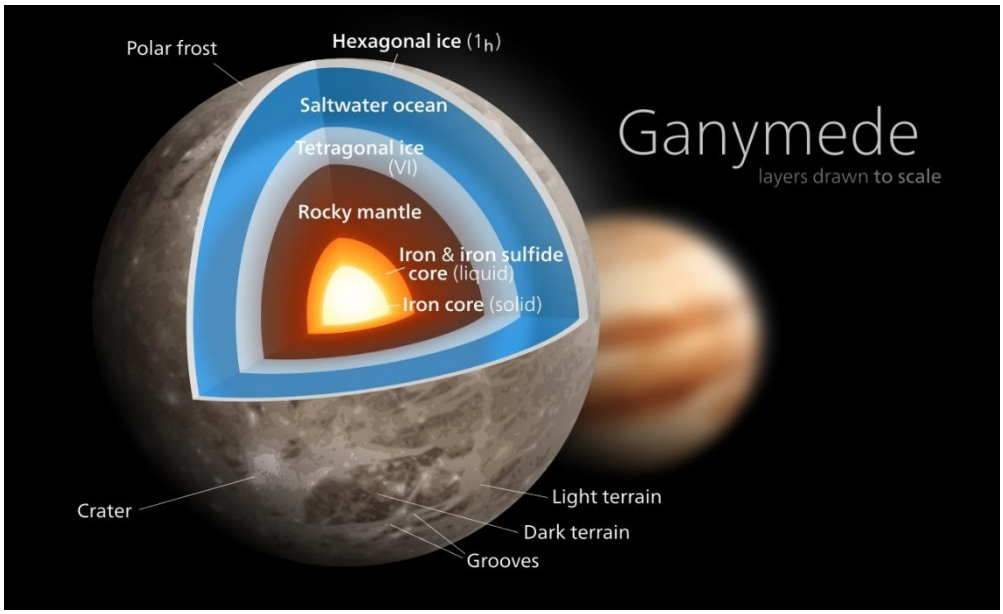


*Figure 1.1:b.* ***GANYMEDE ICY PLANET*** *is the Solar System's largest and most enormous moon, as well as its ninth largest body. It is an ocean moon, too. These planets have a lot of water, either on the surface or under the surface. They are a rocky world that is either coated in liquid water or has an ice layer on top of it. According to the picture, the interior structure is like that of a rocky planet, and there are many different ice and water layers on top of the silicate mantle/crust (Williams, 2015).*

elements like Si, Mg, Fe, and O. Other forms of planets can be habitable and Earth-like in several ways. Enceladus and Europa share the unusual feature of having an ocean that is in contact with a rocky interior, as does Earth. Geophysical measurements (magnetic field and gravity field) by the Galileo and Cassini missions (Wagner, 2014), on the other hand, strongly suggest the presence of water underneath the icy crusts of Calisto, Ganymede, Europa, Titan, and Enceladus, prompting many studies on the possibility of ocean-dominated exoplanets. According to the reports, this study will focus on modelling a typical structure of ocean/icy exoplanets that can be applied to icy exoplanets. So far, the research team has used various bulk compositions, equations of state (EoS),

and other modelling information to investigate mass–radius relations for water-rich exoplanets. In this paper, we construct an interior structure model to infer the interior characteristics of icy exoplanets.

### 1.2 Mass – Radius Relationship

Today, with a certain precision, the interior structure and composition of the Earth are known. Several parameters such as mass, polar and equatorial radii, moment of inertia, geoid, tidal, love numbers, wave seismic velocities, etc. are useful in our cause. Space missions have gleaned similar information to other solar systems up to Saturn. Flight-by missions have shown accurate masses for distant planets such as the Uranus and Neptune, as well as more information on direct imagery (Fischer, et al., 2011).

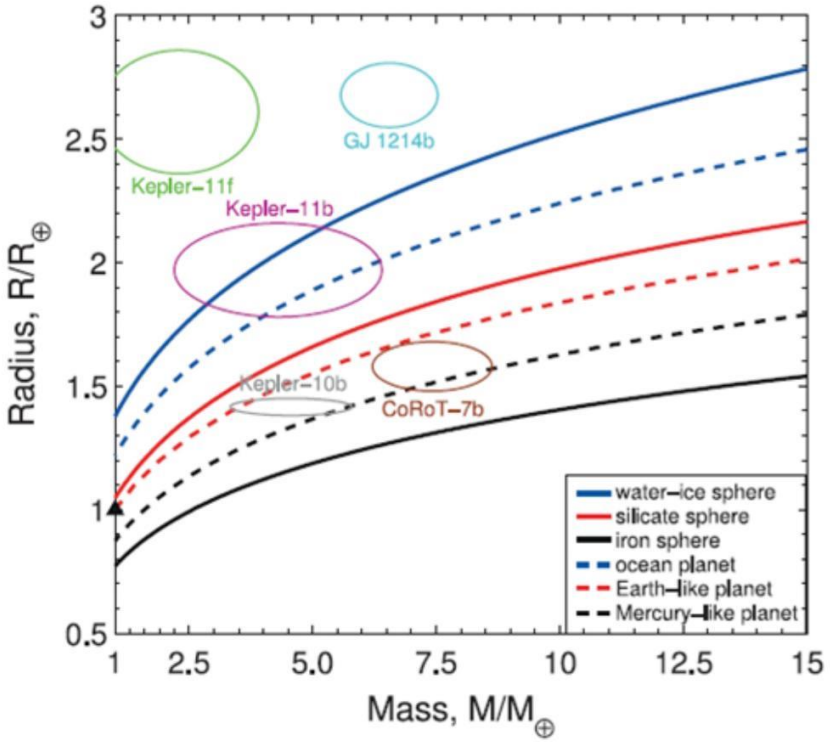


*Figure 1.2:a. Mass-Radius relationship of super-Earths versus observed super-Earths (Wagner, 2014).*

In the case of exoplanets, unfortunately, such services are not available to us. But it is possible to have good estimates of the radius and mass of exoplanets by the transit and radial velocity method..

The relationships with mass radius help to classify the super Earths according to their bulk composition. The help of these interactions to interpret observed super-Earths is shown by Figure

1.2.1 from (Wagner, 2014). A hypothetical water-ice curve represents the blue solid curve, a red shattered curve that is Earth-like, while the black lined curve is for Mercury-like planets. Somewhere between Earth and Mercury, Kepler-10b is expected to have a composition. Kepler-11b, however, appears to have a lot of water ice. For example, if two planets have the same mass but different radii, the smaller planet with a larger core is expected to have an excess content of iron. As per this relationship, Kepler-11f can be identified as a water ice planet since over the higher radii, the total mass seems very low on it.

## 1.3 Chemical and elemental abundance

### 1.3.1 *Super Earths and Exoplanets*

The class of exoplanets, which have masses between the masses of the Earth (1 M) and Neptune (17 masses of earth), could have an earth like a composition, but different pressures and temperatures by means of interior design and structure (Valancia, et al., 2007). Terrestrial exoplanets with masses of 1-10 earth masses are defined as super earths. Thus, its radius from the Kepler mission varies from 1,25 earth radii to 2 earth radii. Whether for terrestrial planets the icy exoplanets can be identified by the same composition in the different measurements of mass radius. Earth's basic composition is dominated by O, Fe, Mg, and Si, which make up more than 95 percent of the total mass. These elements are in good agreement with the abundance of solar elements. These elements are expected to be the primary constituents of exoplanets, regardless of stellar abundances. The super-Earths could then have a composition that is identical to that of the Earth which means technically similar abundance can be used under exoplanet interior including the H20 (Ice or water layers). In addition, their interiors will have two critical layers: core and mantle. Since then, they've enormous planets have more distinct internal layers, and their interior temperatures are higher. This allows the iron-rich alloy to percolate down to the core, resulting in a silicate-rich alloy in mantle and iron rich cores. The overall silicate versus iron ratio can still vary. The super Earths might be more Earth-like (32.5 wt.% iron, 67.5 wt.% silicates) or Mercury-like (70 wt.% iron, 30 wt.% silicates) (Hakim, 2014).

### 1.3.2 *Bulk composition and* chemical formation

The main aspects of planetary interior modelling are composition and structure. There is further discussion of the compositional and structural modelling of exoplanets. Although Earth is made from the same cloud of dust and gas that brought the sun into being, it gradually takes on other findings were interpreted. A large part of H, He, solar wind, and radiation pressure have evaporated it. Heavy elements such as Fe fall to the bottom of the proto-Earth mould cavity, and lighter elements such as Si and O rise, separated by gravity (Stevenson, 2012). The core is therefore rich in iron and the mantle is rich in silicate. Its development resulted in different layer levels of elements. On the contrary, planetary structure composed mainly 8 elements which are O, Si, Mg, Ni, Ca, Al, Fe and S amounting 99% of whole. Stellar abundance is coming up as the main hypotheses of modelling exoplanet interiors since all the data analysis comes under spectroscopic experiments. Nevertheless, the most probable constituent elements for any of those structures are above mentioned chemicals.

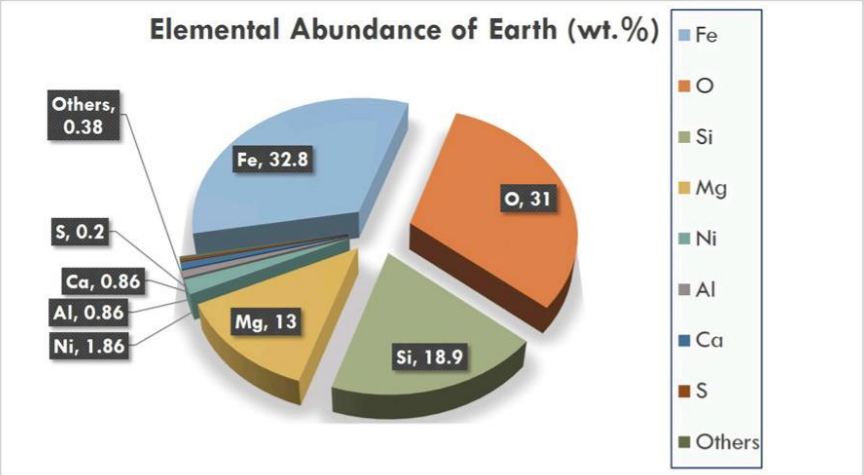


*Figure 1.3:a.* ***Elemental abundance of earth,*** *the chemical elements iron, oxygen, magnesium, and silicone are the most prominent substances which is basically cover 95.7% of the total mass of earth. Altogether with rest of misc. Ions, Ni, Ca, Al these abundance delegate overall 99.3% of composition. Under these conditions' terrestrial planets, the super earths, exoplanets can be identified with these elements under different percentages* (Javoy, 1995).

The mantle in massive oxide fraction, Cao, FeO, MgO, $Al_2O_3$ and $SiO_2$, known collectively as CFMAS are often described by terrestrial planet studies. The less abundant Ca is like Mg, and clinopyroxene is formed in the top mantle of the Earth and calcium perovskite in the lower mantle (Stevenson, 2012). This is caused by an increase in internal pressure. Al in silicates replaces Si

and Mg. It is therefore possible, without affecting chemical performance, to add Ca and Al to other elements. Ni forms a Fe alloy in the core and has similar thermoelastic properties. High layers of less than 24GPa include peridotite compounds. (Clinopyroxene, Garnet, Spinal, Olivine) As super earths or exoplanets that can have pressure differences than earth, thickness of the layers and the material ratios can be varied.

Perovskites, which have a variable formula $(Mg_xFe_{1-x})_2SiO_4$, are the most common silicate material along the stellar abundance. The various pressure peridotites can lead to the formation of perovskites or post perovskites. Composition with chemicals should be defined better than using elemental abundance which is basically more accurate (Sotin, et al., 2007). Thus, the silicate core fraction or bulk composition is common to assume. By changing the core mass fraction, models for various planetary subclasses can be generated. For example, in Mercury-like planets, the earth-like models can have a core mass fraction of 32.5% compared to 70%. In comparison to the Earth, models like Mars and Moons might have smaller core.

### 1.3.3 *Different* compositions layer wise

Mg is the only one of the four main elements that can be integrated into the silicate mantle. As a result, Mg is not mentioned in the sense of centre. Iron alloys make up the cores of the planets in our solar system. Fe and small quantities of Ni make up the Earth's inner solid core, while Fe and light elements make up the outer liquid core (Javoy, 1995). The thermoelastic properties of nickel are identical to those of iron, so it can be safely ignored in the calculations. Iron alloy candidates in Earth's outer core include elements such as S, Si, O, C, and H, but there is no agreement on their choice or number. According to some reports, S is limited to 3% in the earth core but up to 16 % in Mars-like cores. These points apply to other terrestrial planets as well. Because of its preference for Fe-Ni alloy at high pressures, recent studies predict that S, rather than O or Si, would be a primary component of super-Earth iron cores. It also could reduce the melting temperature of Fe (Dziewonski & Anderson, 1981). For the simulation of solar system bodies, determining the composition in the centre is important. However, due to a lack of thermoelastic data for Fe-S alloy, such a task is currently not feasible in the very high-pressure range (>1TPa) of super-Earths. S is also not one of the four elements considered. As a result, its existence in the iron core is ignored.

Since the amount of other light elements trapped in the core of exoplanets cannot be limited, only iron is used to model the core.

The mantle makes up two-thirds of the Earth's total mass. The mantle is dominated by CFMAS compounds. Though the exact composition of the mantle is unknown, it can be estimated that it is made up of 46 % silicon oxide, 38 % magnesium oxide, 8% iron oxide, and trace quantities of other compounds. It is significant to mention that the mantle's composition is determined by major element oxides, such as Si, Mg, and Fe. Peridotite, a rocky stone, makes up the upper layer of the Earth's mantle. The dominant species in the earth's upper mantle is olivine, which contains some iron and has the variable formula $(Mg_xFe_{1-x})_2SiO_4$. (Murakami, et al., 2004)

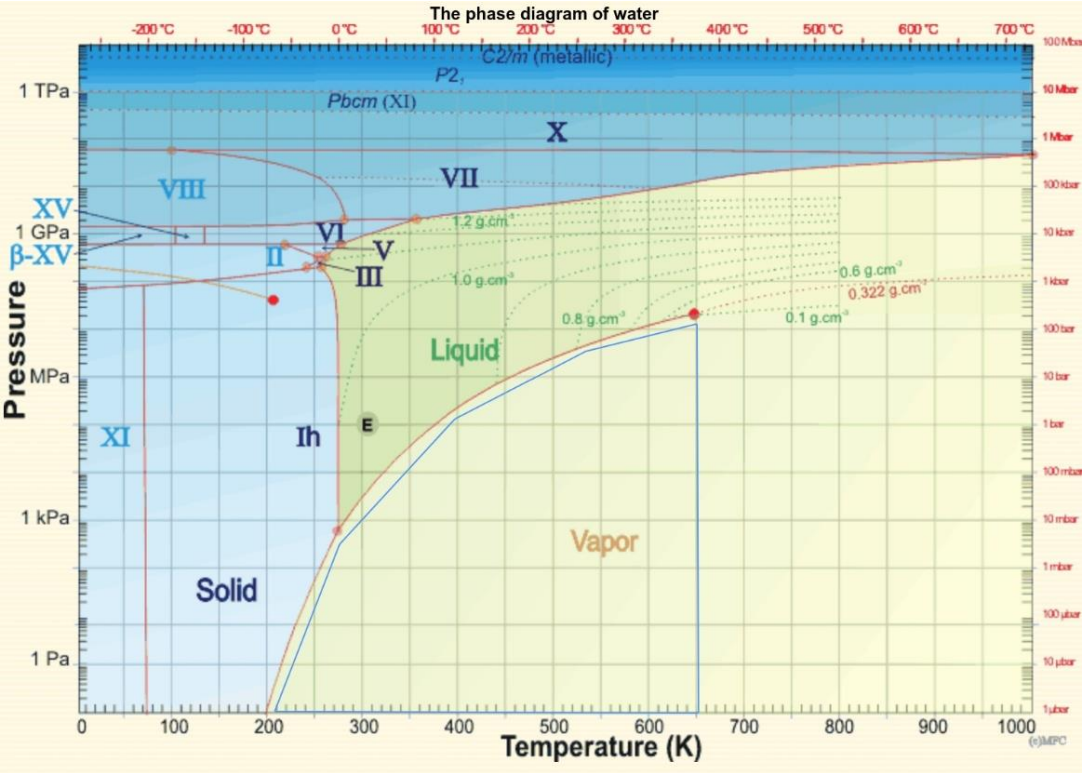


*Figure 1.3:b.* ***Phase diagram of ice/water,*** *this diagram simply can be used to identify which type of ice phase can be consist of the top of the mantle or MCB or crust, according to the final pressure, temperature data points (Chaplin, 2011).*

The thickness of the upper mantle where these minerals occur is predicted to be comparatively small in comparison to the mantle scale as super-Earths pressure increases. The total mass of super-Earths would not be affected by minor differences in the densities of olivine and other minerals. As a result, the upper mantle composition of super-Earths can be assumed to be $(Mg_xFe_{1-x})_2SiO_4$.

A large variety of igneous, metamorphic, and sedimentary rocks make up the Earth's crust. These rocks are a lot lighter than peridotites. Its basic composition differs slightly from that of the mantle minerals. The layer to be exposed to the outside world is the crust. However, crust may or may not

exist to induce icy exoplanet structures. It still contains important ice layers or various phases of layers. On the top of planets $H_2O$ or $CH_4$ are the most prominent ice types. Up a different high-pressure layer of water-ice could be placed on the silicate mantle with different ice phases in this case for the ice planets. (Ice I, Ice VII, Ice IX).

### 1.4 Equation of State

Under high pressure and temperature conditions, materials undergo phase transitions, which affect their density and, as a result, the radius of the planet, as previously stated. As a result, knowing the correct density and thermoelastic properties of a material at relevant pressures and temperatures is crucial. The equations of state (EOS) relate pressure and temperature to matter density, which is the first principle of quantum mechanics. The interaction of molecules, atoms, ions, and electrons, as well as electron degeneracy, can add to their uncertainty. In laboratory experiments, high pressure phases of silicate minerals and solid iron were observed up to pressures of 200GPa. Calculations based on quantum mechanics first principles are used for higher pressures. EOS are critical in determining the interior structure of planets and are currently a bottleneck in super-Earth modelling in the high-pressure regime.

The equation of state (EoS) is a mathematical formula that relates pressure and temperature to matter density. Birch-Murnaghan is the third order EoS where widely used in geographical applications, with the most successful EoS being used to model Mars, Mercury, and some satellites. It also benefits the earth's mantle. The third order Birch-Murnaghan EoS is given by (Birch, 1947)

| EOS | $\rho_0$ (kg /m$^3$) | $V_0$ (cm$^3$ /mole) | $K_0$ (GPa) | $K'_0$ | $K'_\infty$ | $\theta_0$ (K) | $\gamma_0$ | $\gamma_\infty$ | β [or q] |
|---|---|---|---|---|---|---|---|---|---|
| **BM** | 4150.2 | 24.45 | 251 | 4.1 | - | 905 | 1.57 | - | 1.1(q) |
| **Keane** | 3977.6 | 25.24 | 267.7 | 4.04 | 2.6298 | 1114 | 1.506 | 1.1482 | 7.0247 |
| **gen. Rydberg** | 3977.6 | 25.24 | 270.6 | 3.81 | 2.6298 | 1114 | 1.506 | 1.1482 | 7.0247 |
| **Reciprocal K'** | 4145.0 | 24.22 | 234.0 | 4.0 | 2.4107 | 1114 | 1.454 | 1.0387 | 4.460 |

*Table 1.4:a.* ***The thermoelastic data of Mg-perovskite (MgSiO3, pv) for different EOS****, for low pressure regions in upper mantle and crust perovskite thermoelastic data can be used. Basically, these values are accurate for low*

*pressure ranges below 200GPa which means all the laboratory conditions have confirmed these values according to Birch Murnaghan EoS (Hakim, 2014).*

*Equation 1. 3rd order Birch-Murnaghan Equation of State*

$$P = \frac{3}{2}K_0(x^7 - x^5)\{1 + \frac{3}{4}(K_0' - 3)(x^2 - 1)\}$$

$x = (V/V_0)^{1/3}$ *or* $(\rho/\rho_0)^{1/3}$ is a cube root of dimensionless volume. P is the pressure, $K_0$ is the bulk modulus and $K_0'$ is the first derivative with pressure at ambient temperature (Birch, 1947). BM equation of state does not work under extrapolate conditions beyond 200GPa. In terms of BM EoS, however, extrapolation beyond 200GPa is extremely uncertain. (Rivoldini, et al., 2013)

| EOS | $\rho_0$ (kg /m$^3$) | $V_0$ (cm$^3$ /mole) | $K_0$ (GPa) | $K'_0$ | $K'_\infty$ | $\theta_0$ (K) | $\gamma_0$ | $\gamma_\infty$ | $\beta$ [or q] |
|---|---|---|---|---|---|---|---|---|---|
| **BM** | 4110.3 | 24.42 | 231 | 4.0 | - | 855 | 1.89 | - | 1.1(q) |
| **Keane** | 4105.9 | 24.45 | 197.66 | 4.818 | 2.561 | 1100 | 1.553 | 1.114 | 4.731 |
| **gen. Rydberg** | 4105.9 | 24.45 | 204.03 | 4.201 | 2.561 | 1100 | 1.553 | 1.114 | 4.731 |

*Table 1.4:b.* ***The thermoelastic data of Mg-post-perovskite (MgSiO3, ppv) for different EOS.****, for slightly high-pressure regions in lower mantle post-perovskite thermoelastic data can be used. Basically, these values are accurate for low pressure ranges below 200GPa which means all the laboratory conditions have confirmed these values according to Birch Murnaghan EoS. These values suit on ice/water script using 3rd order Birch-Murnaghan as the EoS (Hakim, 2014).*

EoS derived from first principle is obtained at higher P ranges. So, there is a tricky case on developing a proper EoS lies on the pressure range in between 200GPa and 10Tpa since the pressure inside super earth is expected to be gone beyond 1TPa. (Valancia, et al., 2007)

AIMD (ab initio molecular dynamics – basically using approximations to solve Schrodinger's equations rather than empirical information about the molecular systems) based on the Density Functional Theory method were used to calculate the EOS of solid iron states. This approximation method used to acquire conditions which cannot be used in laboratory standards (above 200GPa pressure values). (Cottenier, et al., 2002 - 2013 (2nd edition)) As previously stated, EoS was derived for high pressures using the first principle of quantum mechanics. They can withstand pressures of up to 1.5TPa. The total pressure for the relaxed structure at any given density and

temperature is calculated in AIMD simulations. Anharmonic effects and electronic contribution, on the other hand, are directly included in total pressure calculations. (Holzapfel, et al., 2001)

*Equation 2. Harmonic effect/term of thermal pressure (Pressure approximation) (Belonoshko, et al., 2008)*

$$P_{harm} = {}^{3nR\gamma}/_{V}\left(\frac{\theta}{2} + \frac{\theta}{(e^{\theta/T} - 1)}\right)$$

*Equation 3. Anharmonic and electronic pressure approximation (Bouchet, et al., 2013)*

$$P_{ae}(V,T) = \frac{3R}{2V} m a_0 x^{3m} T^2$$

Bouchet EoS claims to be more formally appropriate than traditional Birch-Murnaghan or Vinet EOS due to the very high-pressure range under study. Holzapfel EOS is given by. (Holzapfel, et al., 2001)

*Equation 4. Holzapfel EoS*

$$P_{holz}(V) = 3K_0 x^{-5}(1-x)\{1 + C_2 x(1-x)\}e^{[C_0(1-x)]}$$

We assumed that the planetary core is made entirely of iron (Fe), and that depending on temperature and pressure, it can have both a solid and liquid portion. The solid portion is most likely made of iron in a hexagonal close-packed (hcp) structure, which is the most stable up to 8TPa. We used an Equation of State to calculate the thermoelastic properties of materials in each layer at high pressure and high temperature (EoS). To calculate the thermoelastic properties of solid iron, we used the EoS and associated parameters described as Bouchet EoS. The Bouchet formulation was shown to reproduce experimental data better than the other Equations of State at P > 200GPa. (Bouchet, et al., 2013)

| **EOS** | **$\rho_0$ (kg /m$^3$)** | **$V_0$ (cm$^3$ /mole)** | **$K_0$ (GPa)** | **$K'_0$** | **$K'_\infty$** | **$\theta_0$ (K)** | **$\gamma_0$** | **$\gamma_\infty$** | **$\beta$ [or q]** |
|---|---|---|---|---|---|---|---|---|---|
| **BM** | 8171 | 6.835 | 135 | 6.0 | - | 998 | 1.36 | - | 0.91 (q) |
| **Vinet** | 8300 | 6.728 | 160.2 | 5.82 | - | 998 | 1.36 | - | 0.91 (q) |

| | | | | | | | | | |
|---|---|---|---|---|---|---|---|---|---|
| **Keane** | 8269.4 | 6.753 | 164.7 | 5.65 | 5.65 | 430 | 1.875 | 1.305 | 3.289 |
| **g. Rydberg** | 8269.4 | 6.753 | 149.4 | 5.65 | 5.65 | 430 | 1.875 | 1.305 | 3.289 |
| **Reciprocal $K'$** | 7488.3 | 7.458 | 169.82 | 4.983 | 4.98 | 430 | 1.8345 | 1.333 | 3.506 |
| **Dewaele** | 8269.6 | 6.753 | 163.4 | 5.38 | - | 417 | 1.875 | 1.305 | 3.289 |
| **Bouchet** | 8878.4 | 6.290 | 253.84 | 4.719 | - | 44.7 | 1.408 | 0.827 | 0.826 |

## 1.5 Numerical model

The goal of numerical modelling is to determine the interior structure of a planet using valid assumptions. It necessitates the computation of material density at each point on the planet, as well as the parameters (pressure, temperature, gravitational acceleration, mass).

*Table 1.4:c* ***The thermoelastic data of ε-Fe for different equations of state,*** *for the modelling of core layer, thermoelastic data according the Bouchet EoS is going to be used to solve ODEs. (Hakim, 2014).*

The planet's interior is divided into two concentric spherical shells (mantle and core) that are chemically homogeneous. These shells can be modelled individually first, then combined to derive planet properties. Each shell is assumed to be spherically symmetric. It means that the thermodynamic properties of matter are primarily determined by radial distance and do not vary significantly with latitude or longitude. (Hakim, 2014)

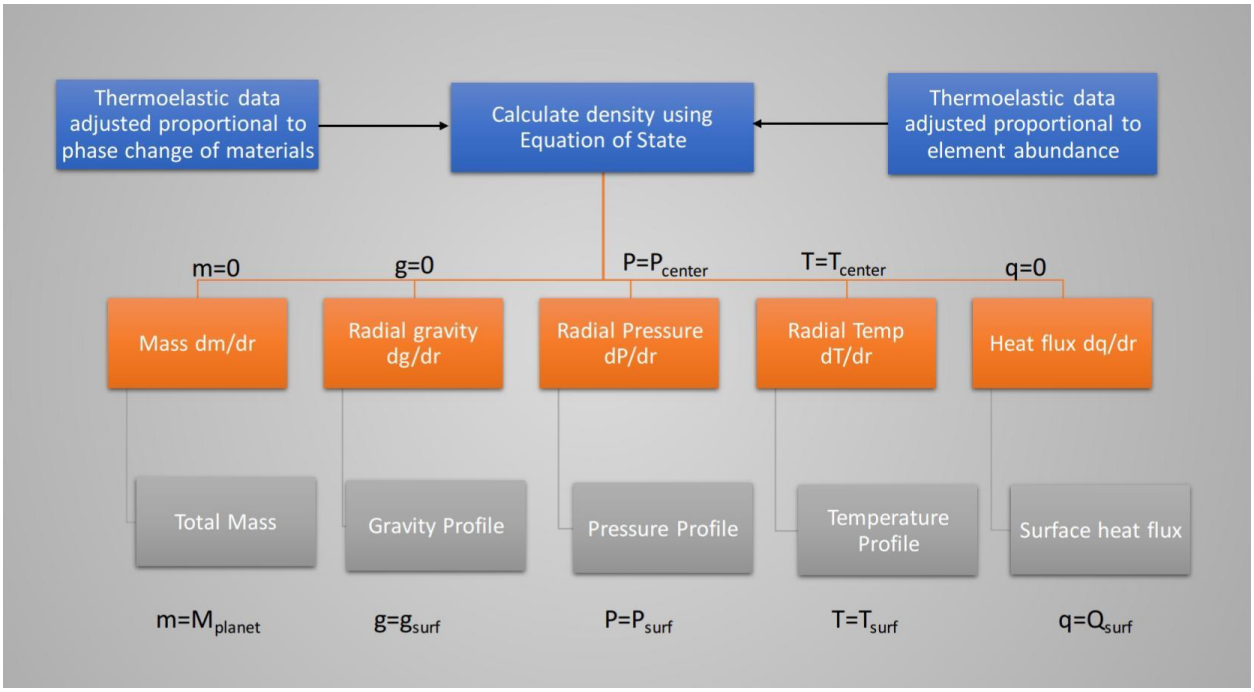


*Table 1.5:a.* ***The modelling strategy is depicted schematically****. Shades of blue represent density calculations, while shades of orange represent ODEs. Each model has two distinct components: composition and structure. They are used as input for the integration of the five ordinary differential equations (ODE), which are radial mass, radial pressure, radial temperature, radial gravity, and heat flux. The five ODEs are solved together by specifying appropriate boundary and continuity conditions. This modelling produces planetary radial profiles of gravity, pressure, temperature, mass, heat flux, and density. In addition, suitable equations of state (EOS) for the mantle, core, and rest must be determined.*

There are several methods for numerically integrating differential equations. To calculate approximate solutions to ODEs, the Runge-Kutta 4$^{th}$ order methods employ variable approximation and iteration. In the Python algorithm, the six ODEs are implicitly solved. Python 3.7 software was used to run this algorithm. Depending on the situation, this programmed script employs one or more of these methods. Before computing the solution, these equations must be supplied with appropriate EOS and thermoelastic data.

# 2 Methodology

Transit photometry is a commonly used way of discovering and studying exoplanets as previously discussed. This scenario in combination with the sensitive photometer is used to detect the exoplanet. Field data include measurements in radial velocity of exoplanet minimum weights and observations in transit of planet radii, thus revealing information on both masses and radius of the inner structure of exoplanets.

The composition and radial profile of the density (rho), pressure (P), temperature (T) and gravity (g) is being investigated using mathematical modelling to deduce the interior structures o Exoplanets, which is the main objective. The P, T, g, and rho profiles of the interior are determined using the Pressure Density Ratio derivative at the appropriate temperature measured from the Equation Of state (EoS). At a certain pressure and temperature within a planet, the deduction process starts with EoS. Under the circumstances, the methodology is developed in various steps. We examine the composition of bulk and we find the most appropriate model to determine interiors specific to the icy Exoplanets. So, the method basically comes up with modelling an interior structure design and calculation of mass-radius relations for several classes of icy exoplanets under construction of bulk composition and numerical modelling. (Herath, et al., 2020)

### 2.1 Bulk composition and phase transition

Bulk composition, as the first aspect, occurs when successive EoS regards are assigned to quantify the key properties in terms of numerical modelling. Even if the Earth was formed from the same cloud of dust and gas as the Sun, it was gradually changed. The solar wind and radiation pressure evaporated substantial amounts of H, He, and other hazardous substances. Fairly substantial elements like Fe sank to the ground, while lighter elements like Si and O rose to the top. Several different hypotheses were made to obtain the primitive data for the measurements as the exoplanet gradually acquired the different composition. (Allegre, et al., 2002) In a molten proto exoplanet, heavier metals like Fe (iron) and Ni fall to the core's bottom, while lighter metals like Si (silicon) and oxygen rise to the mantle's body and crust. To complete the numerical calculations, bulk modules, thermal coefficient, and the rest of the primary data are obtained under these assumptions. (Cottenier, et al., 2002 - 2013 (2nd edition))

Each planetary structure is divided into three parts: the upper olivine component, the perovskite shell, and the pure iron core. With this common structure either rocky/terrestrial planet or icy planets can be divided. On behalf of identifying icy exoplanets, we use end temperature profile at the top of the olivine component. There can be a dissociation in post perovskite at higher temperatures and pressure prevalence in deep interiors in the perovskite zone (Umemoto, et al., 2006). Since we are just looking at the silicate mantle, the dissociation of post perovskite will not have a major effect on the radial mass distribution. (Grocholski, et al., 2010)

Elemental abundance assumes that it is the same as stellar abundance. For example, earth-like planets may have a core mass fraction of about 0.3, compared to 0.7 for Mercury-like planets. Since we are looking for ice exoplanets, we changed the core mass fraction at the same time to get the most likely chemical abundance. So, we looked at Ganymede, an ocean planet with 0.45 water ice, 0.485 silicate, and 0.065 iron, which is close to Jupiter's icy moon. (Wagner, 2014)

An additional high-pressure water-ice layer is built on top of the silicate mantle in the case of icy planets. Because of their minor effects on the mass radius relation, low pressure phase transition within the ice in distribution can be ignored. In addition to the core mass fraction, the water mass fraction is also listed in icy planets at the end of the day.

## 2.2 Numerical Modelling

The radial variation in density, pressure, gravitational acceleration, and temperature is computed using the numerical model. To do so, the planet's interior was divided into concentric shells, including the core, mantle (upper and lower), crust, and ice cap. To determine the radial variant of each property, these shells are presumed to be spherically symmetric and differentiated. Differential equations were used to quantify these properties.

*Equation 5. Radial pressure differential equation.*

$$dP/dr = -\rho g$$

*Equation 6. Radial gravitational acceleration differential equation*

$$dg/dr = 4\pi G\rho - 2(g/r)$$

*Equation 7. Radial mass differential equation*

$$dm/dr = 4\pi r^2 \rho$$

- $r =$ Radial distance from the centre of the planet
- $G =$ Gravitational constant
- $\rho =$ Local density (computed with an equation of state)
- $m =$ Local mass

In here the hypotheses is that each shell is a convection layer and that the temperature varies adiabatically with depth. The adiabatic temperature gradient is given by,

*Equation 8. Radial temperature differential equation*

$$dT/dr = -\gamma/\varphi \, gT$$

- $\gamma =$ Thermodynamic Grüneisen parameter
- $\varphi = K_s/\rho$ $(Both\ parameters\ are\ obtained\ by\ evaluation\ of\ EoS)$
- $K_s =$ Related to adiobatic bulk modulus
- $K_T =$ Related to isothermal bulk modulus
- $K_s = K_T(1 + \gamma\alpha T)$
- $\alpha =$ Coefficient of thermal expansion

A thermal boundary layer with a conductive profile exists between the core and the lower mantle. The core mantle boundary (CMB) has a steeper temperature gradient than the convective layer, resulting in a large temperature jump between the core and the mantle. A conducting layer can be found between the mantle and the crust, as well as within the crust itself. The temperature gradient and heat flux that passes through each layer of conductivity. (Rivoldini, et al., 2013)

*Equation 9. Conducting layer radial temperature differential equation*

$$dT/dr = -q/\kappa$$

*Equation 10. Conducting layer radial heat flux differential equation*

$$dq/dr = \epsilon\rho - 2\,q/r$$

- $\epsilon =$ Specific heat production rate $(7.38 \times 10^{-11} \mathrm{W k} g^{-1}) -$ $matches\ present\ earth\ like\ value$
- $\kappa =$ Thermal conductivity

The thermal conductivity of each layer is referred to as kappa in this case. For large terrestrial exoplanets, the conductivity of the CMB is unknown. As a result, the kappa must be adopted as a constant based on derived conductivity values within the planet. CMB kappa needs to be between 9 and 13 $Wm^{-1}$. The conductivity of the earth's lithosphere, especially the crust, was between 3 and 7 $Wm^{-1}$. Using these values as examples, we set the kappa value for the MCB to 8 & 6 $Wm^{-1}$. (Herath, et al., 2020)

A mathematical formulation relating pressure and temperature to the density or volume of matter is known as an equation of state. The EoS defines a material's bulk properties at a given pressure and temperature. We use the pressure contribution of an EoS for an EoS and the thermal contribution of an EoS for a given material in these models. In case we are using Bouchet form of EoS since its more accurate at 200GPa to 10TPa inside the core. (Bouchet, et al., 2013)

Local density is calculated by,

*Equation 11. Local density calculation using function of temperature and pressure EoS.*

$$\rho(r) = f_{EoS}(P_{(r)}T_{(r)})$$

Where $f_{EoS}$ is the equation of state (EoS), a unique function relating density, pressure, and temperature of a given material in thermal equilibrium. Almost all EoS are semi-empirical fits to high-pressure experiments or seismological observations.

The Bouchet formulation was shown to reproduce experimental data better than the other Equations of State at P > 300GPa. The Bouchet EoS is defined by a static (zero temperature) pressure term as well as three temperature dependent pressure terms that account for harmonic, anharmonic, and electronic contributions. The EoS P (V, T) can then be written as follows. (Bouchet, et al., 2013)

*Equation 12. Equation of state pressure calculation*

$$P(V,T) = P_{harm}(V) + P_{th}(V,T) + P_a(V,T) + P_e(V,T)$$

P (V) is an independent function of temperature and the rest of the parameters provides temperature dependent contribution to the equation of state. The zero-temperature term for solid part starting from the core can be shown using the Holzapfel equation given belove,

*Equation 13. Holzapfel EoS used in Bouchet form.*

$$P_{holz}(V) = 3K_0x^{-5}(1-x)\{1 + C_2x(1-x)\}e^{[C_0(1-x)]}$$

With,

- $x = ({}^{V_0}/_{V})^{1/3}\ or\ ({}^{\rho}/_{\rho_0})^{1/3}$
- $C_0 = -\ln(3K_0/P_{FGO})$
- $P_{FGO} = 1003.6({}^{Z}/_{V_0})^{5/3}\ in\ GPa$

- $C_2 = {}^{3}/_{2}\,(K_0' - 3) - C_0$

$V_0$ is the molar volume $cm^3$/mole, Z is the atomic number (in core, it is iron/Fe), $P_{FGO}$ is in GPa, $K_0$ Bulk modulus at reference temperature and pressure, $K_0' = ({}^{dK_0}/_{dP})$. To define $P_{th}$ which is a functional parameter of coefficient of thermal expansion, below $P_{harm}$ and $P_{ae}$ defined.

*Equation 14. Harmonic effect/term of thermal pressure (Pressure approximation)*

$$P_{harm} = {}^{3nR\gamma}/_{V}\,(\frac{\theta}{2} + \frac{\theta}{(e^{\theta/T} - 1)})$$

*Equation 15. Anharmonic and electronic pressure approximation.*

$$P_{ae}(V,T) = \frac{3R}{2V} m a_0 x^{3m} T^2$$

Mantle script and ice/water phase script basically comes up with Birch- Murnaghan EoS instead of Buchet form of EoS since at higher layers the pressure sensitivity according to the BM is accurate. (Below 200GPa the accuracy of BM3 EoS is adequate) (Hakim, 2014)

*Equation 16. 3rd order Birch-Murnaghan Equation of State.*

$$P = \frac{3}{2} K_0 (x^7 - x^5)\{1 + \frac{3}{4}(K_0' - 3)(x^2 - 1)\}$$

With,

- $x = ({}^{V_0}/_{V})^{1/3}\ or\ ({}^{\rho}/_{\rho_0})^{1/3}$

In those scripts, the 3rd order Birch-Murnaghan EoS is used under pressures belove 200GPa. (Birch, 1947)

Collaborated with the defined EoS parameters, density function calculated through the algorithm and certain data values obtained in terms of 6 different ODEs (Ordinary Differential Equations). Thermoelastic data for relevant EoS is obtained through predetermined values from literature which is consecutive to the element/ion. To measure density using EoS, thermoelastic data should be adjusted proportionally to the material's phase changes, which means it should also be adjusted to the elemental abundance. Each equation of hydrostatic equilibrium, such as mass, radial gravity, radial pressure, heat flux, and radial temperature, should be combined using the density derived

from the equation of state for each layer of the planet when determining bulk properties. Complete mass, gravity profile, pressure profile, surface heat flux, and temperature profile will be obtained by integrating the above equations of hydrostatic equilibrium. (Herath, et al., 2020)

Main method that is used to quantify these properties by integrating the differential equations and obtain relation of pressure, temperature, mass, and density with the radius is Runge-Kutta method of $4^{th}$ order. These numerical operations are done by preformed python algorithm. By obtaining pressure, temperature and gravity profiles respect chemical and elemental abundance have been done and the structure has been developed. We used the brentq function in Python to solve for x as pressure points along the radial distance from the centre to the surface were equated to the EoS. The solution to x was used to find K and compute ρ and V at a given point. The BM3 EoS was solved to find and V for high pressure ices and water. The temperature-dependent volume and density were calculated using these values as inputs. The values of ρ and K were then used as inputs for each ODE, which were numerically combined using a Runge-Kutta algorithm of fourth order. For the inner core, outer core, lower mantle, and upper mantle, we used adiabatic temperature profiles. We used conductive temperature profiles for the CMB, MCB, and crust.

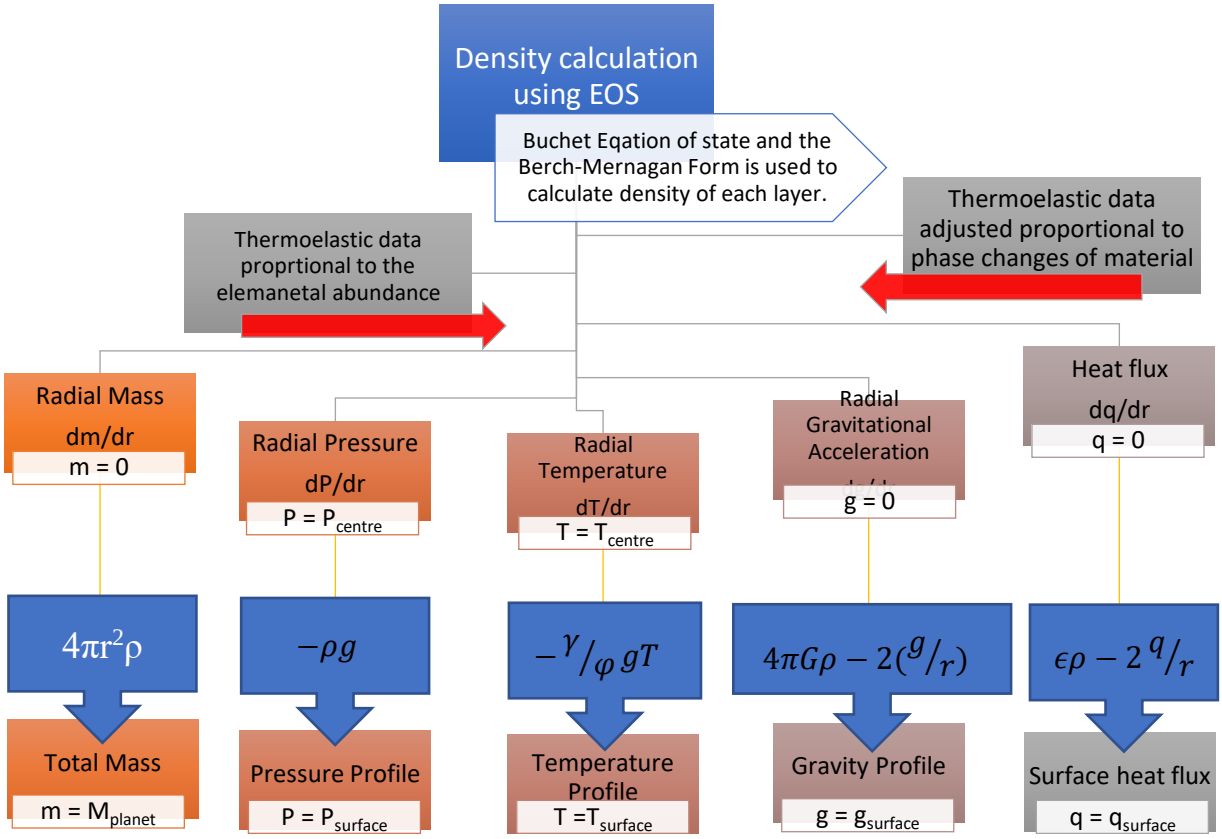


# 3 Results

## 3.1 Rocky Planetary Models

The python script is being tested with known planet data, to check the precision and accuracy of the script and generated models.

### *3.1.1 Completed script for Earth. 4.4.1*

| | | | |
|---|---|---|---|
| P initial | 440.00 GPa | P Final | 1.362197781245626 GPa |
| T initial | 5600.00 K | T Final | 558.5478618763 K |
| | | Radius | 6181.950000018 Km |
| | | Mass | $5.975909568224 \times 10^{24} Kg$ |
| CMF | 0.32 | | |

*Table 3.1:a. Completed model for earth structure.*

### *3.1.2 Completed script for Venus.*

| | | | |
|---|---|---|---|
| P initial | 380.00 GPa | P Final | 0.284595976988206 GPa |
| T initial | 5000.00 K | T Final | 804.5857227060972 K |
| | | Radius | 5751.10000001003392 Km |
| | | Mass | $4.881753685282449 \times 10^{24} Kg$ |
| CMF | 0.32 | | |
| P initial | 380.00 GPa | P Final | 0.262808716874065 GPa |
| T initial | 5000.00 K | T Final | 789.8546518427352 K |
| | | Radius | 5997.3000001004288 Km |
| | | Mass | $5.289644009110386 \times 10^{24} Kg$ |
| CMF | 0.28 | | |

*Table 3.1:b. Completed two model's data for Venus structure.*

Two different CMF values have been tested due to varies research aspects on Venus interior structure. Both graphical interpretations on Venus interior structure is discussed on section Modelling rocky model for earth, Mercury, Venus, Mars. (Accuracy of model)

## 3.2 Ice Planetary Models

To model the interior structure, several different Temperature and Pressure initial values were tested with the python script. All models consist of 0.32 core mass fraction which is more likely to earth CMF. All our models are suits for earth like icy exoplanets, other variants are discussed in section 4. (Modelling rocky model for earth, Mercury, Venus, Mars. (Accuracy of model)).

### *3.2.1 Completed script 01. (Figure 4.3:)*

| | | | |
|---|---|---|---|
| P initial | 350.00 GPa | P | 0.04994878120366424 GPa |
| T initial | 3000.00 K | T | 1174.7428506713275 K |
| | | Mass | $4.413253536837657 \times 10^{24} Kg$ |
| Beginning of ICE | CMB, MCB | Radius | 6286.520001060218 Km |

| | | | |
|---|---|---|---|
| Ending | Water | | |

*Table 3.2:a. Ice model 01, properties*

### *3.2.2 Completed script 02. (Figure 4.3:)*

| | | | |
|---|---|---|---|
| $P_{initial}$ | 360.00 GPa | P | 0.049945496606670206 GPa |
| $T_{initial}$ | 4000.00 K | T | 14.788671183356783K |
| | | Mass | $4.26221560470764 \times 10^{24} Kg$ |
| Beginning of ICE | Lower Mantle 1, MCB | Radius | 5919.2400010234915 Km |
| Ending | Water | | |

*Table 3.2:b. Ice model 02, properties*

### *3.2.3 Incomplete Script 01. Incomplete Ice model 01. (Table 3.2:c. Ice model 03, properties (incomplete))*

| | | | | | |
|---|---|---|---|---|---|
| $P_{initial}$ | 350.00 $GPa$ | Values after MCB | | ICE 8 Script | |
| $T_{initial}$ | 3000.00 $K$ | P | 22.833461409942203 $GPa$ | P | - |
| | | T | 235.30517448778497 $K$ | T | - |
| Beginning | LM2 → MCB | Mass | $3.19555818627376 \times 10^{24} Kg$ | Mass | - |
| Ending | ICE 8 | Radius | 4636.0000009991545 $Km$ | Radius | - |

*Table 3.2:c. Ice model 03, properties (incomplete)*

This model did not complete up to the upper layer of ice. There is no ice 8 python script developed due to lack of thermoelastic data and inadequate evidence in high pressure ice details. Therefore, we could not be able to acquire neither EoS nor thermoelastic data which regards to build up ice 08 phase python script. Incomplete Ice model 01. (Table 3.2:c. Ice model 03, properties (incomplete))

## 3.3 Icy exoplanet and Rocky planet Comparison.

| Rocky planet |
|---|

| | | | |
|---|---|---|---|
| $P_{\text{initial}}$ | 440.00 GPa | $P_{Final}$ | 1.884991396596903 GPa |
| $T_{\text{initial}}$ | 6000.00 K | $T_{Final}$ | 827.345382411258 Kelvin |
| | | Radius | 6016.500001004358 Km |
| | | Mass | $5.492528868140798 \times 10^{24}$ Kg |
| CMF | 0.32 | | |
| Ice planet | | | |
| $P_{\text{initial}}$ | 450.00 GPa | $P_{Final}$ | 0.09920570697421896 GPa |
| $T_{\text{initial}}$ | 6000.00 K | $T_{Final}$ | 797.8904845568727K |
| | | Radius | 6112.1000010047055 Km |
| Beginning of ICE | Upper mantel − MCB − Ice 7 | Mass | $5.574692505973152 \times 10^{24}$ Kg |
| CMF | 0.32 | | |

*3.3:a. Icy exoplanet, Rocky planet comparison chart.*

This comparison done to figure out whether it is Icy or Rocky planet only by looking at the Icy model. Which means the mass-radius relationship can be developed with these models to identify if it is a terrestrial or Rocky planet of Icy planet.

# 4 Discussion and conclusion

## 4.1 Assumptions of chemical composition and bulk composition with respect to each layer.

### *4.1.1 Chemical composition in* core layer

Based on data collected for mass, it is highly likely that the composition of our solar system's earth and other terrestrial planets will be similar. The core, mantle, and upper ice layers make up the interior layers of icy exoplanets. The core is made of iron with a few alloys mixed along (Ni). However, because the thermoelastic data for Fe-alloys are not well besides high pressures, we

ignored the effect of alloys and assumed the core was entirely made of Iron. Based on the melting curve for Fe, the core can be divided into a solid inner core and a liquid outer core. We only considered the solid inner core during our experimentation.

### 4.1.2 *Chemical composition* in mantle

For the lower mantle, we used $MgSiO_3$, $FeSiO_3$, $CaSiO_3$, $Al_2O_3$, MgO, and FeO. At pressures above 130GPa and temperatures above 2000 K, $MgSiO_3$ and $FeSiO_3$ exist in the post-perovskite phase (ppv) (Dziewonski & Anderson, 1981). We are using separate scripts to overcome this ppv phase transition at high pressures by using different thermoelastic values in each script. It is demonstrated that both minerals transform into perovskite (pv) between 130GPa and the transition point of the lower to upper mantle (Murakami, et al., 2004). We assumed that the Mg and Fe Silicates in the upper mantle and crust are dominated by $Mg_2SiO_4$ and $Fe_2SiO_4$, also known as Olivine. The upper layer of the Earth's mantle is made up of peridotite, a rocky material. It is composed of various mineral species such as olivine, orthopyroxene, clinopyroxene, spinel, garnet, and others. The dominant species in the Earth's upper mantle up to pressures of 24GPa is olivine, a magnesium orthosilicate containing some iron with the variable formula $(Mg_xFe_{1-x})_2SiO_4$. As our models reach pressures of several Tera Pascals, we expect the thickness of the upper mantle where these minerals exist to be relatively thin. As we assumed, minor variations in the densities of olivine and other minerals will have no effect on the total mass of model. Although in upper mantle, assumptions can be made as the composition of the layer filled with the olivine part.

### 4.1.3 *Chemical* and bulk composition in ice/water layer

If significant amounts of volatiles are present, the upper or lower mantle will directly transit to the ice layer. These layers are composed of high-pressure ices such as Ice-X, Ice-VII, and Ice-VI, as well as an ocean above them. In the script, third order BM EoS is used to model the ice shells. The thermal expansivity was measured using EoS as described above (Birch, 1947). There were no equations available to determine Ice X's heat capacity. We assumed that Ice VII and Ice X have identical thermal properties. Related to these thermoelastic properties (Javoy, 1995). Ice VII and Ice X were thought to have the same thermal properties, and data for thermal expansivity, conductivity, and heat capacity were included. As a result, we have agreed to apply these properties to every Ice X shells. The thermoelastic properties of ice are given in *(6.1:f. Thermoelastic properties of different elements according to the Chemical abundance of the planet. These values*

*are used to obtain bulk properties on EoS solving. (Assumptions of chemical composition and bulk composition with respect to each layer.))* to find the pressure and temperature dependent properties of liquid water. (Herath, et al., 2020)

#### 4.1.4 *Bulk composition assumptions*

To model the interior, we needed Fe/Mg, Si/Mg, Ca/Mg, and Al/Mg mole ratios, in addition to Mg. For planets with icy upper layers, a water mass fraction was also required. The Fe/Mg ratio of a planet can be used to calculate its Core Mass Fraction (CMF). (Morard, et al., 2011) Because we assumed that the core contained only iron, we calculated CMF using the ratio of Mg, Fe composition on the mantle to Fe component in core value. In this case, we will use 0.32, which is more likely to be the CMF of the Earth. (Wagner, 2014)

### 4.2 EoS and its pressure ranges, alternative EoS and the benefits over them.

The high-pressure tests are gradually improving. In the lab process, the highest pressure that could be reached is currently just over 200GPa. The upper and most of the lower mantle of Earth now have detailed phase equilibria. However, phase equilibria near the Earth's core-mantle boundary (where post-perovskite is discovered) are still being investigated. The largest mineral species in the mantle of exoplanets is post-perovskite, which is used in exoplanet modelling. (Murakami, et al., 2004)

There have been suggestions that advancements in the evaluation of higher density post-perovskite phases have been made. The experimental thermoelastic data will allow for precise determination of material density at extremely high pressures.

Modelling is difficult not only for ppv, but also for core iron composition, due to a lack of knowledge on high pressure EoS. We are modelling the core with the Bouchet form of EoS, and the mantle and higher ice layers with the 3rd order BM EoS. Extrapolation for high pressures above 200GPa, or the 4th order type of EoS, using the BM EoS, is highly uncertain to obtain thermoelastic data for the purpose of solving density profiles. (Hakim, 2014) As a result, the Bouchet form formed under AIMD density functional theory is far superior. So, in this case, we are just using Holzapfel EoS in pressure ranges greater than 300GPa. (Holzapfel, et al., 2001) The remainder of the high-pressure EoS needed to be thermally corrected such like *Universal Equation of state, Generalised Rydberg form of equation of state.* Even Rydberg form of EoS can extrapolate

without any uncertainty to the infinity pressure, still it causes but complexity on the python script due to its thermal correction. Thus far, the beat solution for modelling core was the Bouchet EoS since its very accurate at pressure ranges in between 300GPa to 10TPa. (Hakim, 2014)

## 4.3 Readings

Each ice models, graphical representation according to its Pressure and Temperature profile is being evaluated under this section. Consequently, the obtained graphs, according to each model using python script are given below.

### *4.3.1 Completed Ice model 01 (Table 3.2:)*

For the end mass and radius which can be acquired from any of exoplanet detecting, spectroscopic method this model could be applied. For those implementations, the chemical abundance and elemental abundances are included and with the exact end values this model may suits or any other model can be derived under this algorithm. Considering this model 01; this ice structure concluded solid iron core, core mantle boundary and soon after MCB the water layer exists. Practically for

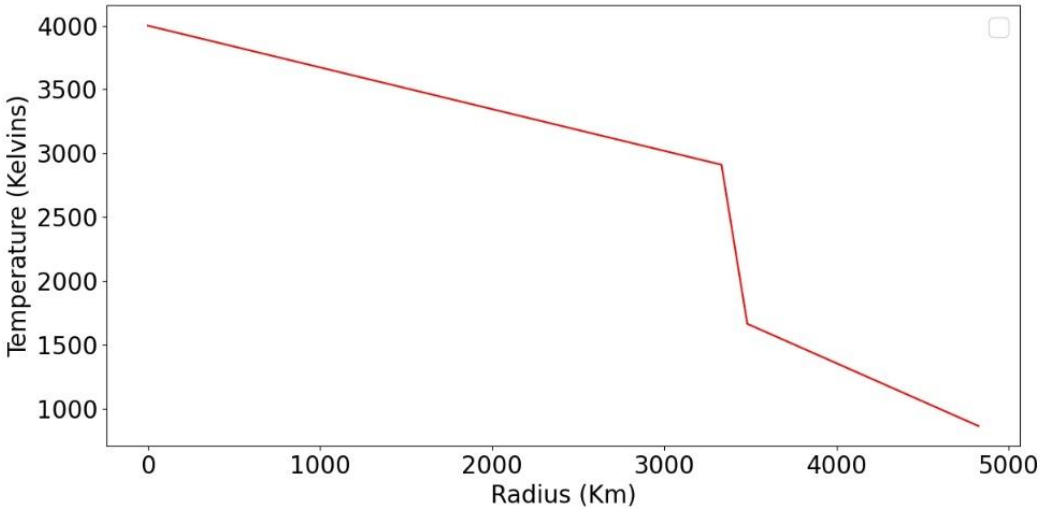


*Figure 4.3:a. Temperature profile for completed ice model 01.*

any water layer existence, a silicon/perovskite layer should have to be remains. But this is not a certain incident, thus far the model could be applied under specific conditions as provided in the results section. (Table 3.2:)

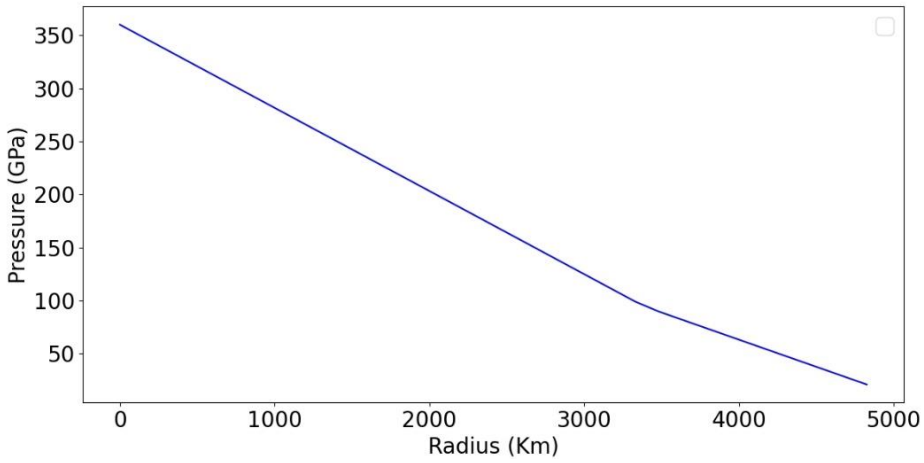


*Figure 4.3:b. Pressure profile for completed ice model 01.*

### *4.3.2 Completed Ice model 02. (Table 3.2:)*

This model (Table 3.2:) ends up same as the above with water layer. As a general model, the structure consists solid iron core, CMB, Lower mantle 01 layer, MCB and then water layer. As on Figure 4.3: ice layer performs sudden drop on temperature curve.

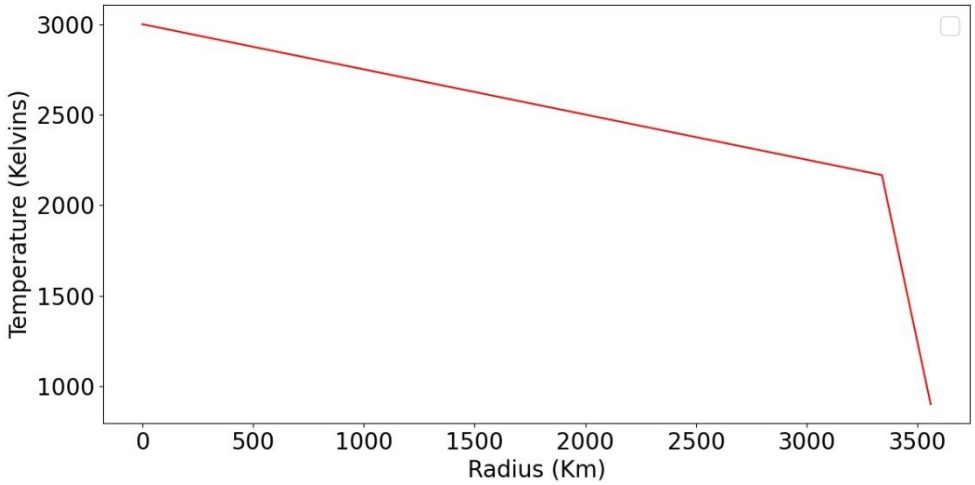


*Figure 4.3:c. Temperature profile for completed ice model 02.*

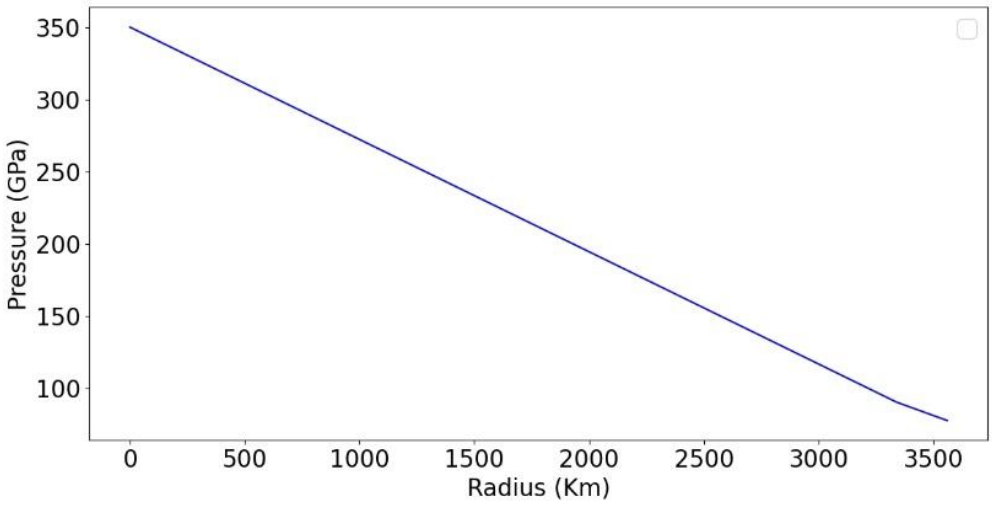


*Figure 4.3:d. Pressure profile for completed ice model 02.*

As per the basics, model consists of perovskite layer soon after the water layer which means that this model can be used as a typical model for icy exoplanets. (Herath, 2021)

#### *4.3.3 Incomplete Ice model 01. (Table 3.2:c. Ice model 03, properties (incomplete))*

Ice 8 phase script is not developed.

#### *4.3.4 Ice model and Rocky model comparison. (**Error! Reference source not found.**)*

Comparison

## 4.4 Modelling rocky model for earth, Mercury, Venus, Mars. (Accuracy of model)

#### *4.4.1 Earth interior structure test. (Completed script for Earth. 4.4.1)*

According to the values in Completed script for , we can justify that our python script is most likely accurate for earth mass range. Because we are modelling the structures of Earth-like icy exoplanets, the end results for appropriate data sets can be considered accurate and consistent

values. Recent ab initio calculations indicate that this $MgSiO_3$ mineralogical phase should be stable up to 1TPa, but its material parameters are debatable and, in comparison to perovskite, less well confined due to the current limitations of high-pressure experiments. The bulk properties model, on the other hand, essentially scales up the current Earth based on seismological evidence, resulting in a truly Earth-like composition. Not only in the mantle, but also in the solid iron core thermoelastic data taken as hypothetical exoplanet properties. As per the EoS we are using and the bulk properties we are assuming, models we are generating pretty much similar in composition to earth. As for the clarification, Venus planetary model also generated with the python script.

*Venus interior structure test (Table 3.1:a. Completed model for earth structure.*

### *4.4.2 Completed script for Venus.*

## 4.5 Improvements on script.

We were received the necessary python script by the Arthur C Clarke Centre, and we developed and modified the script to obtain necessary information on behalf of modelling the icy planets structure.

# 5 Bibliography

Allegre, C. J., Poirier, J. P. & Gillian, M. J., 2002. *Phisics Rev. B.* [Online]
Available at: http://www.sciencedirect.com/science/article/pii/0012821X9500123T
[Accessed 13 May 2021].

Birch, F., 1947. *Finite elastic strain of cube crystals,* s.l.: Harvard Univercity.

Bouchet, J. et al., 2013. *Physics Review B,* s.l.: Science direct.

brenen, P., walbolt, K. & Biferno, A., 2021. *Exoplanet extrapolation, Planets beyond our solar system.* [Online]

Available at: https:/exoplanet.nasa.gov/
[Accessed 26 May 2021].

Chaplin, M., 2011. *Phase transition as a metaphor for the genesis of complexity.* [Online]
Available at: http;//www.webhome.phy.duke.edu/~hsg/763/table-images
[Accessed 10 May 2021].

Cottenier, S., Probert, M. & Hoolst, V., 2002 - 2013 (2nd edition). APW method Step by step introduction. In: S. Cottenier, ed. *Density Functional Theory.* s.l.:s.n., pp. 312,237.

Dziewonski & Anderson, D. L., 1981. *Physics of the earth and planetary interiors,* s.l.: Science Direct.

Fischer, D. A., Howard, A. & Laughlin, G. P., 2011. *Exoplanet Detection Techniques,* s.l.: Science Direct.

Grocholski, B., Shim, S. H. & Prakapenka, V. B., 2010. *Geophysical research letters, 37.* [Online]
Available at: http://dx.doi.org/10.1029/2010GL043945
[Accessed 16 May 2021].

Hakim, K., 2014. *The interior stucture of super earths,* s.l.: KU LEUVEN, Faculty of sciences.

Herath, M., 2021. *Senior Research Scientist.* [Sound Recording] (Arther C Clarke Technological Institute).

Herath, M., Gunasekara, S. & Jayaratne, C., 2020. *Characterization the possible interior structure of the nearby exoplanets proxima centauri b and Ross-128 b,* s.l.: Arther C clarke technological institute.

Holzapfel, W. B., Hartwig, M. & Sievers, W., 2001. *Journal of Physical and Chemical reference data,* Volume 01, pp. 30, 515.

Javoy, M., 1995. *Geophysical Research letters.* [Online]
Available at: http://dx.doi.org/10.1029/95GL02015
[Accessed 6 May 2021].

Javoy, M., 1995. *Geophysical Research letters 22.* [Online]
Available at: http://www.dx.doi.org/10.1029/95GL02015
[Accessed 17 May 2021].

Morard, G. et al., 2011. In: *High energy density physics.* s.l.:s.n., pp. 7, 141.

Murakami, M., K, H. & Katsuyuki, K., 2004. *Science - Post Perovskite transition in MgSiO3.* [Online]
Available at: www.sciencemag.org/science/content/304/5672/855.abstract
[Accessed 10 May 2021].

Murray, B., 2018. *Planetary.* [Online]
Available at: http://www.planetary.org/space-image/interior-structures-of-earth-mars-moon
[Accessed 3 May 2021].

Rivoldini, A., Van Hoolst, V. & Verhoven, 2013. *Erath and planetery Scince letters.* [Online]
Available at: http://www.sciencedirect.com/science/article/pii/s0019103511001151
[Accessed 12 May 2021].

Sotin, Grasette, O. & Moscquet, A., 2007. *Mass radius curve for extra solar earth like planets and ocean planets,* s.l.: Icarus.

Stevenson, D. J., 2012. *Nature.* [Online]
Available at: http://dx.doi.org/10.1038/485052a
[Accessed 5 May 2021].

Umemoto, K., Wentzcovitch, R. M., Weidner, D. J. & Parise, J. B., 2006. *Geophysical Research Letters.* [Online]
Available at: http://www.dx.doi.org/10.1029/2006GL02348
[Accessed 15 May 2021].

Valancia, Sasselov, D. D. & O'Conelle, R. J., 2007. *Radius and the structure models of the Super earth planets,* s.l.: Icarus.

Wagner, F. W., 2014. *Interior structure model of solid exoplanets using material laws in the infinite pressure limit,* s.l.: Elsevire Icarus.

Williams, M., 2015. *Astronomy & Space, Space exploration, Jupiter's moon Ganymede.* [Online] Available at: https://phys.org/news/
[Accessed 5 May 2021].

# 6 Appendix

## 6.1 Incomplete models of exoplanets.

*Due to the pandemic situation of COVID 19 we could not complete most of the icy models we have developed. Because of the travel restrictions and lockdown situation collaboration project could not get updated with Arthur C Clarke Technological Institute. Since we were unable to visit the institute during lockdown period most of our models did not analyse with proof reading. In this section, deficient planet models are uploaded.*

| | | | |
|---|---|---|---|
| $P_{initial}$ | 500 | P | 0.04997510317983137 |
| $T_{initial}$ | 4000 | T | 767.3691406134093 |
| | | Mass | 10.092525255559827e+24 |
| Beginning | Lower mantle → MCB | Radius | 8678.760001056216 |
| Ending | ICE10, WATER | | |

*Table 6.1:a. This model consists ice 10 layer soon after the silicate mantle and then on the top of ice 10 layer there is a water layer. Final physical properties are taken after the end of water layer which means soon after the water layer it may exists atmosphere or else.*

| | | | |
|---|---|---|---|
| $P_{initial}$ | 330 | P | 2.526793363855645 |
| $T_{initial}$ | 3027 | T | 232.68914204106284 |
| | | Mass | 3.448727652115664e+24 |
| Beginning | UM → MCB | Radius | 5001.100000999353 |
| Ending | ICE 6 | | |

*6.1:b. This model starts ice layer from Upper mantle, MCB. This consists Ice 06 layer up to the end of the planet.*

| | | | |
|---|---|---|---|
| $P_{initial}$ | 367.00 | P | 1.5481183464247044 |
| $T_{initial}$ | 3127.00 | T | 214.37840222224077 |
| | | Mass | 4.3934847500548355e+24 |
| Beginning | Lower mantle 1 → MCB | Radius | 6103.8500010037615 |
| Ending | Ice 7 | | |

*6.1:c. Ice layer starts with Ice 07 on this model. This ice 7 layer starts with Lower mantle, MCB layer.*

| | | | |
|---|---|---|---|
| $P_{initial}$ | 320.0 | P | 0.04994435142850346 |
| $T_{initial}$ | 3000.0 | T | 440.6020922448767 |
| | | Mass | 3.4798954506428297e+24 |
| Beginning | Lower mantle 1 → MCB | Radius | 5548.370001019398 |
| Ending | ICE 7, water | | |

*6.1:d. This model ends with ice 07 layer and then water layer. As most of the generated models, this ice layers are start-up with Lower mantle, MCB layer.*

| | | | |
|---|---|---|---|
| $P_{initial}$ | 360.0 | P | 14.3104690535683 |
| $T_{initial}$ | 4000.0 | T | 617.468825142725 |
| | | Mass | 3.693767452413503e+24 |
| Beginning | Lower mantle 1 → MCB | Radius | 5178.200001001308 |
| Ending | ICE 7 | | |

*6.1:e. Model ends with ice 07 layer which starts from Lower mantle, MCB layer.*

| Compound | $\rho_0$ (Kgm$^{-3}$) | $V_0$ (cm$^{-3}$mol$^{-1}$) | $K_0$ (GPa) | $K_0'$ | $\theta_0$ (K) | $\gamma_0$ | $\gamma_\infty$ | $\beta$ |
|---|---|---|---|---|---|---|---|---|
| **Core** | | | | | | | | |
| Fe (solid)[a] | 8878.40 | 6.290 | 253.8 | 4.719 | 44.70 | 1.408 | 0.827 | 0.826 |
| Fe (liquid)[b] | 5210.40 | 10.72 | 24.60 | 6.650 | - | 1.850 | - | 0.826 |
| **Lower mantle** | | | | | | | | |
| $MgSiO_3$(ppv)[c] | 4110.30 | 24.42 | 231.0 | 4.000 | 855.0 | 1.890 | - | 1.100 |
| $MgSiO_3$(pv)[c] | 4105.20 | 24.45 | 251.0 | 4.100 | 905.0 | 1.570 | - | 1.100 |
| MgO (pe)[c] | 3674.20 | 11.24 | 161.0 | 3.800 | 767.0 | 1.360 | - | 1.700 |
| $FeSiO_3$(ppv)[c] | 5029.10 | 25.46 | 231.0 | 4.000 | 782.0 | 1.890 | - | 1.100 |
| $FeSiO_3$(pv)[c] | 5178.50 | 25.49 | 272.0 | 4.100 | 871.0 | 1.570 | - | 1.100 |
| FeO (wu)[c] | 5872.75 | 12.26 | 179.0 | 4.900 | 454.0 | 1.530 | - | 1.700 |
| $Al_2O_3$(ppv)[c] | 4192.87 | 23.85 | 249.0 | 4.000 | 762.0 | 1.650 | - | 1.100 |
| $Al_2O_3$($rh_2$)[c] | 4009.62 | 24.94 | 258.0 | 4.100 | 886.0 | 1.570 | - | 1.100 |
| **Lower and upper mantles + crust** | | | | | | | | |
| $Al_2O_3$(co)[c] | 3909.30 | 25.58 | 253.0 | 4.300 | 933.0 | 1.320 | - | 1.300 |
| $CaSiO_3$(pv)[c] | 4225.86 | 27.45 | 236.0 | 3.900 | 796.0 | 1.890 | - | 0.900 |
| **Upper mantle + crust** | | | | | | | | |
| $Mg_2SiO_4$(ri)[c] | 3562.20 | 34.49 | 185.0 | 4.200 | 878.0 | 1.110 | - | 2.400 |
| $Mg_2SiO_4$(wa)[c] | 3471.70 | 40.52 | 169.0 | 4.300 | 844.0 | 1.210 | - | 2.000 |
| $Mg_2SiO_4$(fo)[c] | 3226.40 | 43.60 | 128.0 | 4.200 | 809.0 | 0.990 | - | 2.100 |
| $Mg_2Si_2O_6$(en)[c] | 3190.81 | 62.68 | 107.0 | 7.000 | 812.0 | 0.780 | - | 3.400 |
| $Fe_2SiO_4$(ri)[c] | 4875.34 | 41.86 | 213.0 | 4.200 | 679.0 | 1.270 | - | 2.400 |
| $Fe_2SiO_4$(fa)[c] | 4406.99 | 46.29 | 135.0 | 4.200 | 619.0 | 1.060 | - | 3.600 |
| $Fe_2Si_2O_6$(fs)[c] | 4033.97 | 65.94 | 101.0 | 7.000 | 674.0 | 0.720 | - | 3.400 |
| **Volatiles** | | | | | | | | |
| Ice-X[d] | 2318.60 | 7.770 | 162.8 | 4.420 | 1470.0 | 1.200 | - | 1.100 |
| Ice-VII[e] | 1460.00 | 12.30 | 23.90 | 4.200 | 1470.0 | 1.200 | - | 1.100 |

*6.1:f. Thermoelastic properties of different elements according to the Chemical abundance of the planet. These values are used to obtain bulk properties on EoS solving. (Assumptions of chemical composition and bulk composition with respect to each layer.)*